Available online at www.sciencedirect.com
ScienceDirect
Journal of Nuclear Materials 360 (2007) 136–142
journal of nuclear materials
www.elsevier.com/locate/jnucmat

Stability of nanometer-sized oxide clusters in mechanically-alloyed steel under ion-induced displacement cascade damage conditions

P. Pareige [a,*], M.K. Miller [b], R.E. Stoller [c], D.T. Hoelzer [c], E. Cadel [a], B. Radiguet [a]

[a] *Groupe de Physique des Matériaux UMR CNRS 6634, Equipe de Recherche Technologique no 1000, Faculté des Sciences, Av. de l'Université, BP12, 76801 St Etienne du Rouvray, France*
[b] *Microscopy, Microanalysis, Microstructure Group, Oak Ridge National Laboratory, P.O. Box 2008, Building 4500S, Oak Ridge, TN 37831-6136, USA*
[c] *Nuclear Materials Science and Technology Group, Metals and Ceramics Division, Oak Ridge National Laboratory, P.O. Box 2008, Building 4500S, Oak Ridge, TN 37831-6136, USA*

Received 1 March 2005; accepted 14 September 2006

Abstract

Oxide dispersion strengthened ferritic steels are being considered for a number of advanced nuclear reactor applications because of their high strength and potential for high temperature application. Since these properties are attributed to the presence of a high density of very small (nanometer-sized) oxide clusters, there is interest in examining the radiation stability of such clusters. A novel experiment has been carried out to examine oxide nanocluster stability in a mechanically alloyed, oxide dispersion strengthened ferritic steel designated 12YWT. Pre-polished specimens were ion irradiated and the resulting microstructure was examined by atom probe tomography. After ion irradiation to ~0.7 dpa with 150 keV Fe ions at 300 °C, a high number density of ~4 nm-diameter nanoclusters was observed in the ferritic matrix. The nanoclusters are enriched in yttrium, titanium and oxygen, depleted in tungsten and chromium, and have a stoichiometry close to (Ti + Y):O. A similar cluster population was observed in the unirradiated materials, indicating that the ultrafine oxide nanoclusters are resistant to coarsening and dissolution under displacement cascade damage for the ion irradiation conditions used.

PACS: 61.80.Jh; 61.82.Bg

1. Introduction

Mechanically-alloyed oxide dispersion-strengthened (MA/ODS) ferritic steels were developed in the late 1970s for liquid–metal fast breeder reactors due to their excellent high temperature creep and

* Corresponding author. Tel.: +33 2 35 14 68 78; fax: +33 2 35 14 66 52.
E-mail address: philippe.pareige@univ-rouen.fr (P. Pareige).

0022-3115/$ - see front matter © 2006 Elsevier B.V. All rights reserved.
doi:10.1016/j.jnucmat.2006.09.011

tensile properties, and further development has continued [1–7]. Their use is also attractive for space nuclear power systems [8] and fusion reactor applications [9]. High fluence neutron irradiation of structural materials typically produces extensive microstructural evolution due to atomic displacements. For some components, the neutron exposure can lead to more than 100 displacements per atom (dpa). The damage is characterized by atomic displacement cascades which produce large numbers of vacancies and self-interstitial atoms, small clusters of these point defects, and about 20 appm He/dpa by nuclear transmutation reactions. The evolution of this defect population at elevated temperatures leads to changes in the dislocation structure, phase instabilities, and phenomena such as void swelling, irradiation creep, and embrittlement by grain boundary He bubbles.

The MA/ODS steel designated 12YWT [Fe–12.3 wt%Cr–3%W–0.39%Ti–0.25%Y_2O_3 {Fe–13.3 at.%Cr, 0.92%W, 0.46%Ti, 0.13%Y and 0.19%O}] was developed by Japan's Kobe Steel and has been particularly well-studied [9–15]. The very high creep strength exhibited by this alloy has been attributed to a high density of very small (~2–3 nm) mixed (Y + Ti) oxide particles that form during the consolidation and post-consolidation heat treatment of the mechanically alloyed powders [11–14,16]. This conclusion is supported by comparisons of mechanical property measurements on alloys made with slight compositional variations that either prevent or lead to nanocluster formation [10]. The size, shape, chemical composition, number densities of the nanoclusters were characterized by atom probe techniques, which are most suitable for obtaining an accurate description of nanoscale features in metallic materials [17,18]. Atom probe tomography examination of the 12YWT alloy in the as-received condition and after isothermal annealing at temperatures up to 1300 °C ($0.85T_m$) for up to 10 h indicated that the nanoclusters are very stable.

Because of the interest in ODS steels for nuclear applications, it is important to determine if the nanoclusters remain stable when exposed to displacive irradiation. Displacement cascades could promote the loss of these particles by ballistic dissolution, and the radiation-enhanced diffusion of solute atoms arising from their coupling with persistent point defect fluxes could also influence particle stability. In addition to providing desirable mechanical strength, a stable nanocluster population could also provide improved resistance to the effects of irradiation by acting as trapping and recombination sites for both point defects and He. Therefore, a novel experiment involving 300 °C Fe ion irradiation of prepared atom probe specimens has been performed in an initial assessment of nanocluster stability in the 12YWT alloy.

Ion irradiation is often used to simulate the effects of neutron irradiation because an appropriate choice of ion type and energy can be used to obtain displacement cascades that are similar to those induced by fast neutron irradiation. Displacement rates are typically two to four orders of magnitude higher than for neutron irradiation. This acceleration can be both an advantage in terms of the time required for the experiment, and a disadvantage in directly extrapolating the results to the lower reactor irradiation conditions. A primary advantage of the ion irradiation technique is simplified handling of materials because no induced radioactivity is obtained. However, the limited range of heavy charged particles means that only the region very near the specimen surface, typically up to a few micrometers depth even for MeV ions, is irradiated. Thus, it is difficult to prepare atom probe specimens from ion irradiated materials. However, since the portion of an atom probe specimen to be analyzed is electropolished to a thickness of typically ~100 nm, it is possible to irradiate the complete analysis volume with a suitable choice of ion energy.

A previous study [19] examined the differences between electron and light ion (He) irradiation in an ODS alloy with much coarser oxide particles. Although the size range and nature of the oxide particles were different than in the 12YWT, those authors observed that He ion irradiation with small displacement cascades did not strongly modify the size of large oxide particles (>50 nm). The shape of the oxide became more rounded and some yttria particles became amorphous. They found that irradiation with 1.2 MeV electrons did lead to a decrease of the size of very large, ~200 nm, oxide particles. Thus, their study indicated ballistic ejection of atoms as not responsible for the observed loss of diameter, and the role of point defect diffusion has to be taken into account.

2. Materials and experimental

The 12YWT alloy was prepared by milling 70 mm-diameter pre-alloyed metal and 20 nm-diameter Y_2O_3 powders in a high energy attritor mill for 48 h under an argon atmosphere. The mechanically alloyed

flakes were then degassed for 2 h at 400 °C in vacuum at a pressure of $<2\times10^{-2}$ Pa, canned in mild steel and then directly consolidated into bar by hot extrusion at 1150 °C. The alloys were hot rolled at 1150 °C into 7 mm sheet, warm rolled at 600 °C to 2.7 mm sheet and then annealed for 1 h at 1050 °C in vacuum [10].

To fabricate the atom probe specimens, $0.2\times0.2\times10\ \text{mm}^3$ bars were cut from the sheet. These bars were electropolished into needle-shaped atom probe field ion microscopy specimens with standard methods [17,18]. The typical end radius of the needles was ~50 nm. This specimen thickness is suitable for *in situ* ion irradiation. Iron ions were selected so as not to introduce any additional chemical or size effects of the implanted species. In order to study the interaction of the ions with the microstructure, the energy of the iron ions was selected so that the damage region was close to the centerline of the atom probe needle. Suitable irradiation parameters were determined using SRIM 2003 [20], and typical ion trajectories and the ion range distribution for 150 keV iron ions is shown in Fig. 1. Since the specimen presents a curved surface slightly inclined to the ion beam, the end-of-range region tracks across the centerline of the specimen. This is illustrated Fig. 2, where the computed 150 keV ion range and analysis volume have been superimposed on a transmission electron micrograph (TEM) image of a typical atom probe specimen. The specimens were irradiated in the medium energy ion accelerator (IRMA) of the Mass Spectrometry and Nuclear Spectrometry Center (CSNSM)-Orsay, France [21,22] with a controlled 150 keV iron ion beam. The irradiation parameters are reported in Table 1. The damage rate is higher, and the irradiation temperature is lower than in many of the irradiation conditions of interest for these ODS alloys.

The atom probe tomography characterizations were performed in the Groupe de Physique des Matériaux (UMR CNRS 6634-ERT1000)'s Tomographic Atom Probe (TAP). The experiments were performed with a specimen temperature of 50–60 K, pulse repetition of 1.5 kHz, and a pulse fraction of 20% of the standing voltage. The atom probe analyses were performed along the centerline of the specimen to sample the ion implanted region. All the compositions quoted in this paper are expressed in atomic percent. The Guinier radius, r_G, and the composition of the particles were determined from the positions of the solute atoms associated with the particles with the use of the maximum separation method. The parameters used were a maximum solute separation distance of 0.6 nm and a grid spacing of 0.1 nm [18].

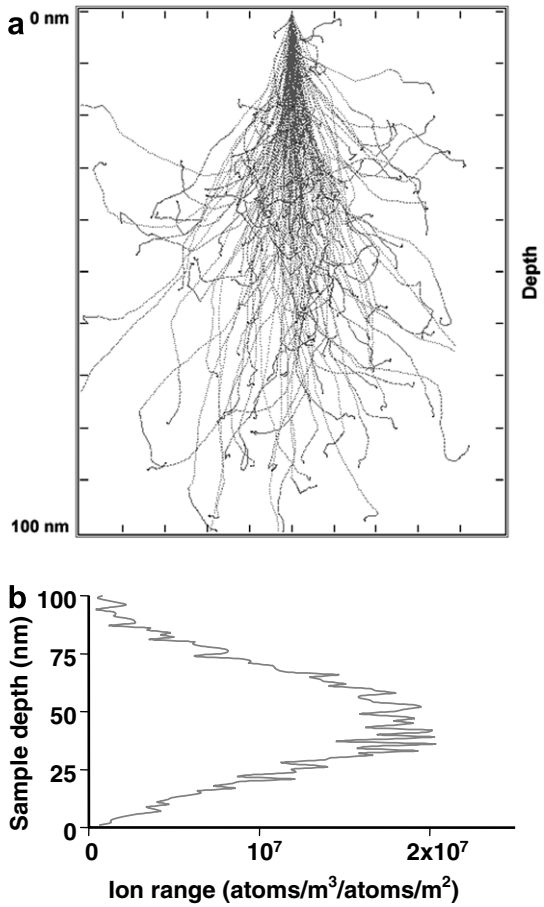

Fig. 1. Results from SRIM 2003 calculation for iron irradiation with 150 keV iron ions. Typical ion trajectories are shown in (a) and the ion range distribution in (b).

3. Irradiation conditions

In order to determine the irradiation damage that occurred in the analyzed volume of the atom probe sample, the number of cascades per unit of time and volume was calculated. The distribution of energies given to primary knock atoms (PKA) as a function of the depth in the atom probe sample is shown in Fig. 3. The PKA distribution is obtained as a function of energy and depth from Fig. 3. The number of PKA at a given depth, p, per second is given by

$$N_{\text{PKA}}^{E,p}/s/\text{at} = \frac{N_{\text{PKA}}^{E,p}\cdot\Phi}{N_{\text{ion}}\cdot N_{\text{at}}\cdot\Delta p},$$

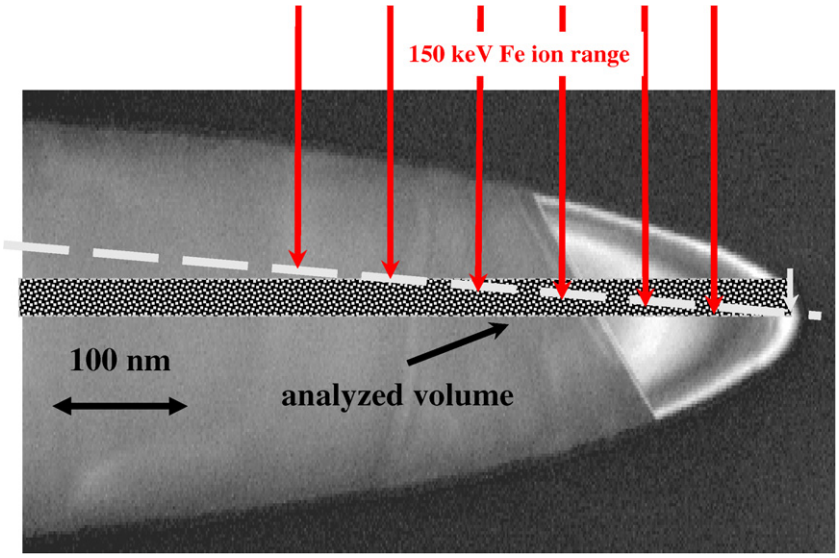

Fig. 2. TEM micrograph of typical atom probe specimen with computed 150 keV ion range and analysis volume superimposed.

Table 1
Ion irradiation conditions for 12YWT alloy

Ion	Energy (keV)	Flux (ion/m^{-2}/s^{-1})	Fluence (ion/m^{-2})	Irradiation time (s)	Damage rate (dpa NRT/s)	Total exposure (dpa NRT)	Temperature (°C)
Fe	150	5×10^{14}	1.8×10^{18}	3600	1.9×10^{-4}	0.7	300

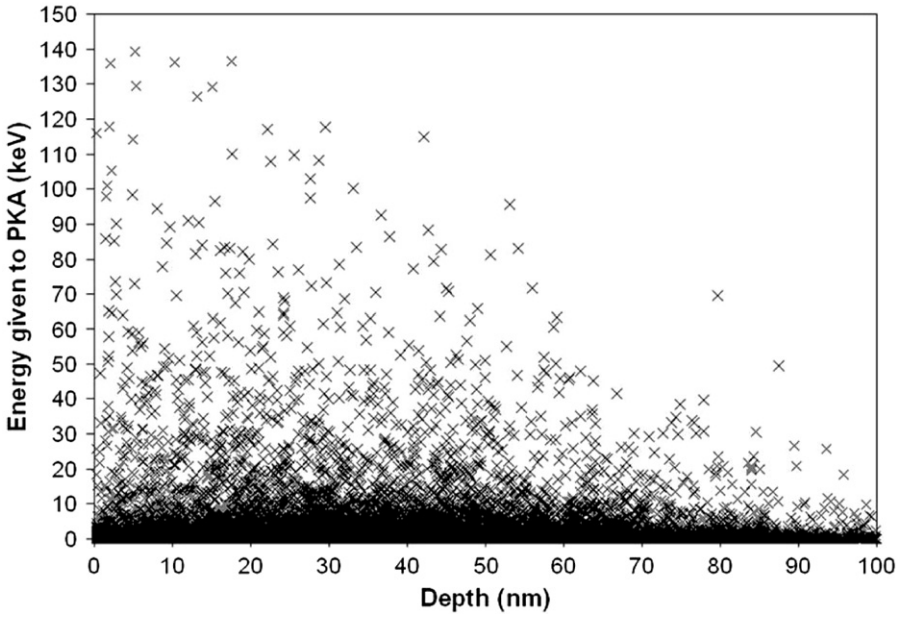

Fig. 3. Energy given to PKA as a function of the depth (or thickness) of the sample with 150 keV Fe-ion irradiation.

where Φ is the ion flux (ions m^{-2} s^{-1}), N_{ion} is the number of incident ions used in the SRIM simulation, Δp is the depth increment and N_{at} is the number of target atoms in a volume: $1\,\text{m}^2 \times \Delta p$. This

distribution contains PKA with energies above 20 keV. Although only a few results are available for the description of such high energy displacement cascades, it is known from previous work [23] that displacement cascades in iron above energies of 20 keV are divided into subcascades. Taking account of that fact, cascades from PKA with energies higher than 20 keV in the previous distribution were replaced in the analysis of the SRIM simulations by their subcascade distributions. Thus, the production rate of displacement cascades or subcascades with energies between 0.1 and 20 keV were calculated at any depth of the sample as shown in Fig. 4. In addition, to have an accurate estimate of the damage in the irradiated, prepolished specimen, the thickness of the specimen needs to be accurately known. These thickness values were obtained by two ways. The prepolished samples were examined in TEM before irradiation. The end radius of the atom probe needle-shaped specimen was also estimated in the three dimensional atom probe from the $R = V/(\beta \times E)$ relationship, where R is the radius (nm), V the applied voltage (kV) to the specimen, β an experimentally determined geometrical constant and E the evaporation field ($V\,nm^{-1}$) [17,18]. The thickness of the sample at its extremity is then twice the end radius of the atom probe needle-shaped specimen.

Under the specified irradiation conditions, the production rate of relatively large displacement cascades or subcascades is taken as the sum of those with energies above 10 keV in Fig. 4, $4.6 \times 10^{22}\,m^{-3}\,s^{-1}$. Thus, in a typical volume of $10^{-23}\,m^3$ ($10 \times 10 \times 100\,nm^3$) analyzed in a 3DAP, one displacement cascade ($10\,keV < E < 20\,keV$) is produced every two seconds. This means that about 1800 displacement cascades were produced in the analyzed volume. Based on displacement cascade simulations such as those in Ref. [23], a typical subcascade radius in α-iron is 2–3 nm. For subcascade radii in this range, the total cascade volume is about 6–20 times the analyzed volume. Therefore, 6–20 displacement cascades have impinged on each individual nanocluster during the 3600 s ion irradiation. The defect production rate in units of NRT dpa/s was also estimated from the SRIM results. The displacement rate in the analyzed volume was found to be 1.9×10^{-4} dpa/s, leading to a total dose of about 0.7 dpa for the one-hour irradiation.

Combining the SRIM calculation with the analysis of molecular dynamics (MD) cascade simula-

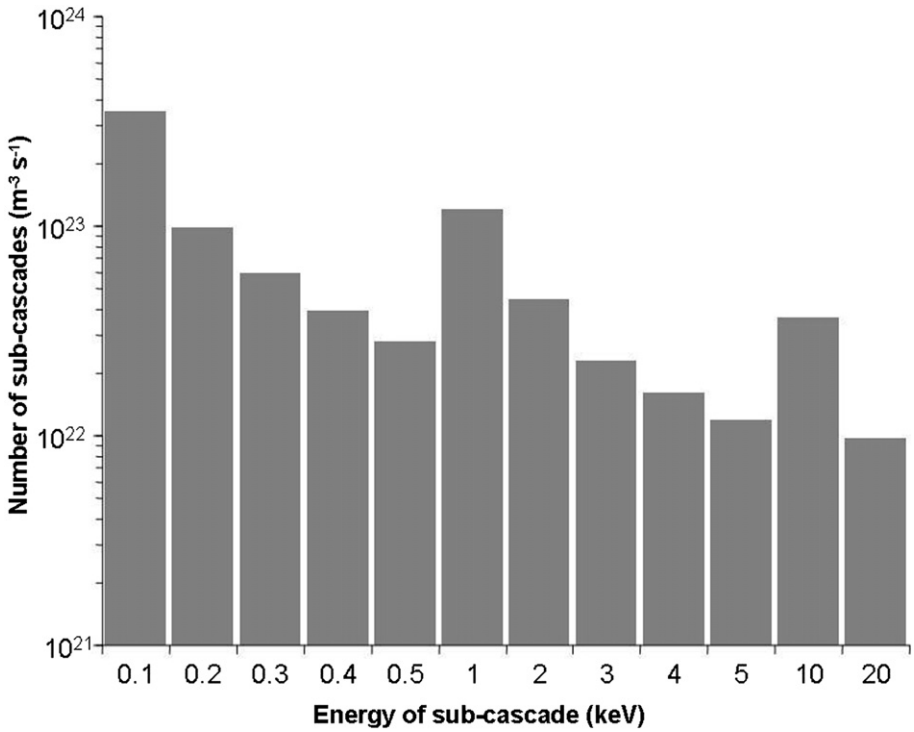

Fig. 4. Subcascade production rate in the analyzed volume of the atom probe sample.

tions to obtain a radiation damage source term, and then employing this source term in a mean field (reaction rate theory model) [24–26], the steady state point defect concentrations produced during the ion irradiation at 300 °C were calculated to be 10^{-7} and 10^{-13} atomic fraction for vacancies and interstitials, respectively. These calculations accounted for the initial displacement cascades, point defect recombination, and point defect elimination at sinks (point defect clusters, dislocations, and the sample surface). The primary damage analysis lead to a point defect production rate of 4×10^{-5} dpa s^{-1}. As expected from MD simulations [23], this value is smaller than the NRT dpa rate obtained from with SRIM.

4. Microstructural observations

The solute distributions observed in two specimens of the 12YWT alloy after Fe ion irradiation at 300 °C are shown in the atom maps in Fig. 5(a) and (b). The analyzed volumes are $14 \times 14 \times 120\ nm^3$ in Fig. 5(a) and $14 \times 14 \times 80\ nm^3$ in Fig. 5(b). Following the analysis described above, about 1800 displacement subcascades with energies above 10 keV have occurred in each volume, but there is no evidence of the nanoclusters dissolving and no coarsening is observed.

The number density of ultrafine Ti-, Y- and O-enriched nanoclusters observed was $\sim 5 \times 10^{23}\ m^{-3}$. The average Guinier radius of the nanoclusters was determined to be 2.0 nm with values in the range 1–3 nm. The number density was slightly below the $1.4 \times 10^{24}\ m^{-3}$ measured in the as-received condition and slightly above the number densities measured in the thermally aged material [14]. Values of 4.3 and $3.8 \times 10^{23}\ m^{-3}$ were measured after annealing for 1 and 10 h at 1300 °C, respectively. The compositions of the particles in atom percent are: 6%Y, 39%Ti, 42%O, and 2%Cr, with traces of W and the balance being iron. The results are consistent with the chemistry ratios observed in the as-received and thermally aged materials; the nanoclusters are enriched in yttrium, titanium and oxygen and depleted in tungsten and chromium and have a stoichiometry close to (Ti + Y):O.

Tomographic atom probe analysis indicates that the high flux ion irradiation which generated many displacement cascades in the vicinity and on the top of the nanoclusters has not lead to: (i) ballistic dissolution, (ii) dissolution due to the production of a high level of freely migrating defects, or (iii) coarsening of the nanoclusters. This irradiation study further demonstrates the extremely high stability of these ultrafine oxide nanoclusters.

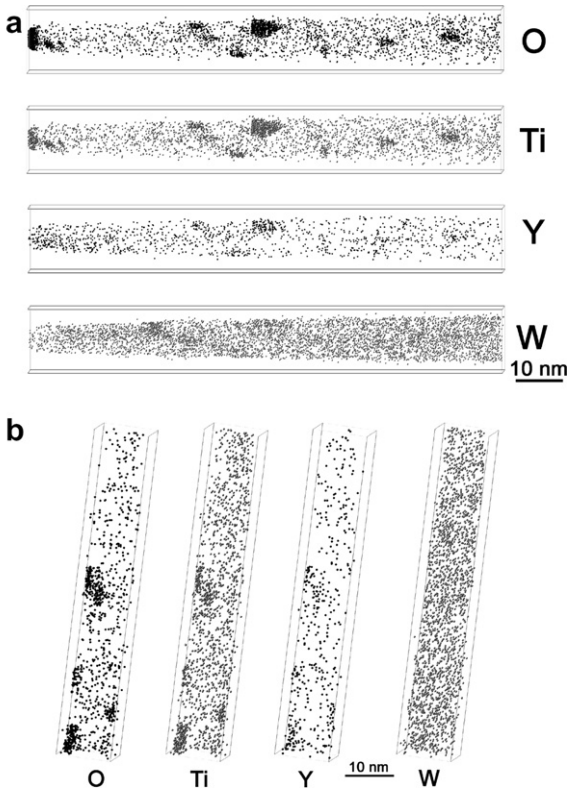

Fig. 5. Atom maps showing titanium-, oxygen- and yttrium-enriched nanoclusters in the 12YWT alloy after Fe ion irradiation at 300 °C. The lines are the three-dimensional box bounding the data. The atom maps in parts (a) and (b) correspond to two different ion irradiated samples.

5. Conclusions

The radiation stability of oxide nanoclusters in the 12YWT MA/ODS ferritic alloy was investigated with by atom probe tomography. After ion irradiation to ~0.7 dpa with Fe ions at 300 °C, a high number density of ~4 nm-diameter nanoclusters was observed in the ferritic matrix. The size, number density, and chemical composition of the nanoclusters were similar to that observed in the as-received and thermally-aged specimens. The large number of energetic displacement cascades that occurred in the analyzed volume of material (1800 displacement cascades in $10^4\ nm^3$) did not lead to either ballistic dissolution of the oxide particles or their coarsening.

This result is in agreement with an earlier study on a different class of ODS alloy mentioned above. The presence of these ultra-fine oxide nanoclusters in the MA/ODS ferritic materials is responsible for their good mechanical performance, particularly high temperature strength by blocking mobile dislocations. The observed stability of the nanoparticles under irradiation is an encouraging indicator for their use in advanced nuclear energy systems, and suggests that the particles have the potential to help reduce phenomena such as void swelling by acting as trapping/recombination sites for point defects produced under irradiation. Further experiments are needed to confirm the desirable behavior at higher irradiation temperatures and doses.

Acknowledgements

Research at the Oak Ridge National Laboratory was sponsored by the Division of Materials Sciences and Engineering, and the Office of Nuclear Energy, Science and Technology, US Department of Energy, under Contract DE-AC05-00OR22725 with UT-Battelle, LLC. The authors thank M.O. Ruault and O. Kaitasov from CSNSM, IN2P3/CNRS, bat 108, 91405 Orsay campus, France, for ion irradiation of the specimen with IRMA implanter.

References

[1] J.J. Fischer, Dispersion strengthened ferritic alloy for use in liquid-metal fast breeder reactor (LMFBRS), U.S. Patent 4,075,010 issued February 1978.
[2] G.D. Smith, J.J. de Barbadillo, Structural Applications of Mechanical Alloying, in: J.J. de Barbadillo et al. (Eds.), ASM-International, Materials Park, OH, 1994, p. 117.
[3] S. Ukai, M. Harada, H. Okada, M. Inoue, S. Nomura, S. Shikakura, K. Asabe, T. Nishida, M. Fujiwara, J. Nucl. Mater. 204 (1993) 65.
[4] S. Ukai, M. Harada, H. Okada, M. Inoue, S. Nomura, S. Shikakura, T. Nishida, M. Fujiwara, J. Nucl. Mater. 204 (1993) 74.
[5] S. Ukai, T. Nishida, H. Okada, T. Okuda, M. Fujiwara, K. Asabe, J. Nucl. Sci. Technol. 34 (1997) 256.
[6] S. Ukai, T. Yoshitake, S. Mizuta, Y. Matsudaira, S. Hagi, T. Kobayashi, J. Nucl. Sci. Technol. 36 (1999) 710.
[7] I.-S. Kim, T. Okuda, C.-Y. Kang, J.-H. Sung, P.J. Maziasz, R.L. Klueh, K. Miyahara, Met. Mater. 6 (2000) 513.
[8] M. El-Genk, J.M. Tournier, J. Nucl. Mater. 340 (2005) 93.
[9] R.L. Klueh, J.P. Shingledecker, R.W. Swindeman, D.T. Hoelzer, J. Nucl. Mater. 341 (2005) 103.
[10] I-S. Kim, B-Y. Choi, C-Y. Kang, T. Okuda, P.J. Maziasz, K. Miyahara, ISIJ International 43 (2003) 1640.
[11] M.K. Miller, E.A. Kenik, K.F. Russel, L. Heatherly, D.T. Hoelzer, P.J. Maziasz, Mat. Sci. Eng. A 353 (2003) 140.
[12] D.J. Larson, P.J. Maziasz, I.-S. Kim, K. Miyahara, Scripta Mater. 44 (2001) 359.
[13] M.K. Miller, D.T. Hoelzer, E.A. Kenik, K.F. Russell, J. Nucl. Mater. 329–333 (2004) 338.
[14] M.K. Miller, D.T. Hoelzer, E.A. Kenik, K.F. Russell, Intermetallics 13 (2005) 387.
[15] M.A. Sokolov, D.T. Hoelzer, M.K. Miller, R.E. Stoller, Fracture Toughness and Tensile Properties of Nanostructured Ferritic Steel, in: D. Hui (Ed.), Presented at Eleventh International Conference on Composites/Nano Engineering, August 8–14, 2004, Hilton-Head Island, South Carolina.
[16] M.J. Alinger, G.R. Odette, D.T. Hoelzer, J. Nucl. Mater. 329–333 (2004) 382.
[17] M.K. Miller, A. Cerezo, M.G. Hetherington, G.D.W. Smith, Atom Probe Field Ion Microscopy, Oxford University, Oxford, UK, 1996.
[18] M.K. Miller, Atom Probe Tomography, Kluwer Academic/Plenum, New York, 2000.
[19] I. Monnet, P. Dubuisson, Y. Serruis, M.O. Ruault, O. Kaitasov, B. Jouffrey, J. Nucl. Mater. 335 (2004) 311.
[20] J.F. Ziegler, J.P. Biersack, U. Littmark, Stopping and Range of Ions in Matter, Pergamon, New York, 1985.
[21] J. Chaumont, H. Bernas, F. Lalu, et al., Nucl. Instrum. and Meth. 189 (1981) 193.
[22] P. Pareige, B. Radiguet, R. Krummeich, A. Barbu, O. Zabusov, M. Kozodaev, Philos. Mag. 85 (2005) 429.
[23] R.E. Stoller, L.R. Greenwood, J. Nucl. Mater. 271&272 (1999) 57.
[24] C. Domain, J. Ruste, Becquart C., Technical Note, EDF, Les Renardieres, September 1999, p. 129.
[25] A. Hardouin Duparc, C. Moingeon, N. Smetniansky-de-Grande, A. Barbu, J. Nucl. Mater. 302 (2002) 143.
[26] B. Radiguet, PhD thesis, Université de Rouen, France, 2004.